Batteries & Supercaps

Perspective
doi.org/10.1002/batt.202500135

Chemistry Europe
European Chemical Societies Publishing

www.batteries-supercaps.org

Insight into the Hybrid Zn–Co/Air Batteries Coupling Faradic Redox and Oxygen Catalytic Reactions

Wenxu Shang, Yongfu Liu, Yi He,* and Peng Tan*

Hybrid Zn–Co/air batteries achieve both high energy density and high energy efficiency by coupling the oxygen catalytic reaction of Zn–air batteries and the Faradic redox reaction of Zn–Co batteries. However, challenges exist in practical applications, including low utilization rate of active material, insufficient oxygen catalytic activity, and unmatched reaction interfaces. These limitations hinder the performance of hybrid Zn–Co/air batteries and restrict their ability in broader application scenarios. This work reviews the recent development of hybrid Zn–Co/air batteries and focuses on their core issues. In terms of active material structure design, advancements are made in microstructure optimization, defect engineering, ion doping, and electrochemical activation. In the area of catalytic activity optimization, improvements are achieved through the optimization of support materials, structural engineering, and defect engineering. In the field of interface optimization, progress has been made in hydrophilicity and hydrophobicity design, gas transfer channel optimization, and electrode structure design. Finally, this work summarizes the future research directions and technical challenges to promote the commercialization of hybrid Zn–Co/air batteries. The in-depth analysis aims to provide valuable guidance to researchers to develop the next-generation high-performance hybrid Zn–Co/air batteries.

1. Introduction

In recent years, alkaline Zn-based batteries have demonstrated significant competitive advantages in energy storage due to the high theoretical specific capacity of Zn (820 mAh g^{-1}), multi-electron transfer characteristics, and the intrinsic safety of nonflammable potassium hydroxide electrolyte systems.[1–3] According to the 2022 U.S. Department of Energy report, the raw material cost of Zn ($1,848/ton) is merely 1/15 of lithium, combined with its high crustal abundance and mature recycling technologies, endowing these batteries with strategic importance for large-scale energy storage applications.[4] Compared with conventional lithium-ion systems, alkaline Zn-based batteries typically exhibit higher operating voltage plateaus (1.4–1.8 V) and faster redox kinetics, primarily attributed to the high ionic conductivity of KOH electrolytes and low polarization characteristics of Zn metal electrodes.[5–7]

Based on system configurations, alkaline Zn-based batteries can be classified into two typical categories: semiopen and fully enclosed systems.[8] The former, represented by Zn–air batteries, employs open-structured gas diffusion electrodes as cathodes to achieve energy storage through oxygen reduction (ORR) and evolution (OER) reactions using ambient oxygen.[9] While this system theoretically achieves an energy density of 1,350 Wh kg^{-1}, practical discharge voltages typically remain below 1.4 V due to limitations in bifunctional catalyst activity and oxygen electrode polarization losses. Notably, conventional Zn–air battery catalysts (e.g., Pt/C, IrO_2) merely serve as reaction interfaces without participating in bulk redox processes, resulting in low utilization of active sites.[10] Fully enclosed systems (e.g., Zn–Ni, Zn–Co batteries) utilize intrinsic redox reactions of cathode materials (e.g., phase transition of NiOOH/$Ni(OH)_2$) for energy storage, demonstrating excellent rate capability and cycling stability.[11] However, constrained by the low theoretical capacity ($Ni(OH)_2$: 289 mAh g^{-1}) and poor conductivity of cathode materials, their energy density struggles to surpass the theoretical limit of 300 Wh kg^{-1}.[12]

To overcome the performance limitations of single-system architectures, researchers have recently proposed innovative hybrid Zn–air battery configurations.[8] This system integrates the intrinsic redox reactions of metal oxides with oxygen electrocatalytic processes through rationally designed bifunctional hybrid cathodes, achieving synergistic enhancement of high voltage platforms and specific capacity.[13] Among various hybrid cathodes, cobalt-based electrodes exhibit unique advantages. First, Co_3O_4 possesses high theoretical capacity (446 mAh g^{-1}) and reversible redox potential (1.8 V vs. Zn), enabling pseudocapacitive fast charge storage; Second, cobalt-based materials demonstrate superior catalytic activity for both ORR and OER; Finally,

W. Shang
Deep Space Exploration Laboratory
Hefei 230088, China

Y. Liu
School of Intelligent Manufacturing
Huzhou College
Huzhou, Zhejiang 313000, China

Y. He
Department of Chemical Engineering
University of Waterloo
Waterloo, Ontario N2L3G1, Canada
E-mail: yi.he@uwaterloo.ca

P. Tan
Department of Thermal Science and Energy Engineering
University of Science and Technology of China
Hefei, Anhui 230026, China
E-mail: pengtan@ustc.edu.cn

P. Tan
State Key Laboratory of Fire Science
University of Science and Technology of China
Hefei, Anhui 230026, China

Perspective
doi.org/10.1002/batt.202500135
Chemistry Europe
European Chemical Societies Publishing

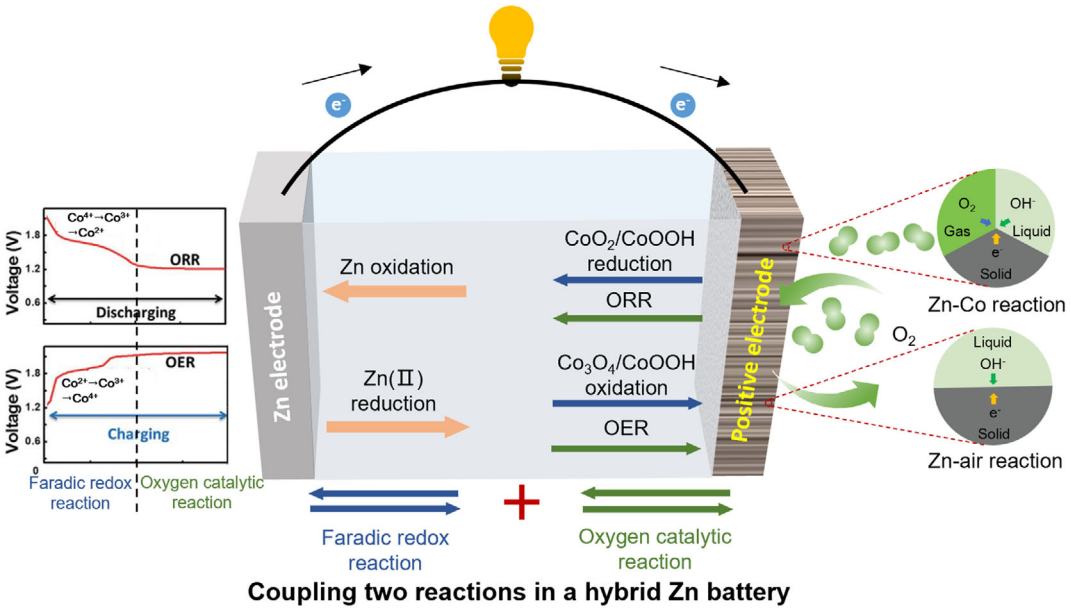

Figure 1. Schematic illustration of the battery structures and working mechanisms of hybrid Zn battery, taking Zn–Co/air batteries as an example.

their spinel structure facilitates the construction of 3D conductive networks to enhance active material utilization, which can be determined as the ratio of actual discharge capacity to theoretical capacity.[14,15] As illustrated in **Figure 1**, during discharge, the reduction of high-valence cobalt species (CoO_2/CoOOH) first provides high-voltage output (>1.6 V) (Equation 1), followed by ORR contributing additional capacity (Equation 2). The charging process involves the oxidation of Co_3O_4/CoOOH and OER. For the Zn electrode, redox reactions between Zn and Zn(II) occur during cycling (Equation 3), establishing a dual-stage energy storage mechanism that simultaneously achieves high energy density and efficiency within a single cell.[16,17] For the discharge process (upper), the Faradic reaction reducing from a high-valence to a low-valence state ($Co^{4+} \rightarrow Co^{3+} \rightarrow Co^{2+}$) first occurs, corresponding to the high-voltage interval. As the active substance gradually turns to a low-valence state, the voltage continues to decrease until the voltage reaches the Zn–air reaction interval. At this time, the positive electrode active substance will act as an oxygen reaction catalyst, which is manifested as a Zn–air section. For the charging process (bottom), the reaction is the opposite. Therefore, the Faradic redox reaction and the oxygen catalytic reaction can work together in the hybrid system.

$$Co_3O_4 + OH^- + H_2O \underset{\text{Discharge}}{\overset{\text{Charge}}{\rightleftharpoons}} 3CoOOH + e^- \quad (1)$$

$$CoOOH + OH^- \underset{\text{Discharge}}{\overset{\text{Charge}}{\rightleftharpoons}} CoO_2 + H_2O + e^- \quad (2)$$

$$Zn(OH)_4^{2-} + 2e^- \underset{\text{Discharge}}{\overset{\text{Charge}}{\rightleftharpoons}} Zn + 4OH^- \quad (3)$$

For the positive electrode of the hybrid Zn–Co battery, it can participate in the reaction as an active substance (corresponding to the Zn–Co reaction section); meanwhile, it can also serve as an oxygen reaction catalyst (corresponding to the Zn–air reaction section). For the Zn–Co reaction section, the actual performance including capacity and energy density depends on the active material structure design. While for the Zn–air reaction section, the charge and discharge efficiency depend on the activity of the catalyst. In addition, the above two reaction interfaces are different (Zn–Co: liquid/solid two-phase interface, Zn–air: gas/liquid/solid three-phase interface), and the interface needs to be reasonably designed to meet the requirement of two reactions. Hence, the practical application of hybrid Zn–Co batteries remains hindered by three critical scientific challenges: low bulk utilization of active materials, insufficient density of oxygen catalytic active sites, and poor solid–liquid–gas three-phase interfaces.[8] Departing from conventional review frameworks, this work focuses on these core issues, systematically analyzing recent breakthroughs in the structural design of active materials, catalytic activity modulation, and interface optimization for hybrid Zn–Co batteries. The comprehensive discussion will provide theoretical guidance and technological pathways for developing next-generation high-energy-density Zn-based energy storage devices.

2. The Electrode Optimization Design

This section will discuss the electrode optimization strategy of the hybrid Zn batteries and the corresponding electrochemical performance (**Table 1**).

2.1. High-Utilization Positive Electrode Design

To improve the utilization ratio of the active material in hybrid Zn–Co batteries, researchers have employed various electrode material optimization techniques, including microstructure

Table 1. Performance of the hybrid Zn batteries based on cobalt electrode.

Positive electrode materials	Electrolyte	Electrochemical performance						Ref.
		Capacity [mAh g_{zn}^{-1}]	Discharging Voltages [V]	Energy density [W h kg^{-1}]	Power density	Cycling stability	Energy efficiency	
Co_3O_4 nanosheets	6 M KOH + 0.02 M zinc acetate	792	1.85 → 1.0	836	41 mW cm^{-2} @24 mA cm^{-2}	200 cycles at 1 mA cm^{-2} (30 min per cycle)	70%	[49]
Co_3O_4 nanowire/Ni foam	6 M KOH + 0.1 M zinc acetate	771	1.6 → 1.05	–	35.7 mW cm^{-2} @68 mA cm^{-2}	1000 cycles at 10 mA cm^{-2} (20 min per cycle)	70%	[16]
Co_3O_4/carbon cloth	6 M KOH + 0.02 M zinc acetate	805	–	936	38.6 mW cm^{-2} @25 mA cm^{-2}	400 cycles at 10 mA cm^{-2} (4 min per cycle)	–	[14]
Co_3O_{4-x} nanorods	6 M KOH with 0.2 M zinc acetate	800	1.90 → 1.23	1060	3200 W kg^{-1} @80 mA cm^{-2}	1500 cycles at 1 mA cm^{-2} (- min per cycle)	>75%	[50]
$NiCo_2O_4$/NiF@C	6 M KOH + 0.2 M zinc acetate	688	1.7 → 1.2	–	26.2 mW cm^{-2} @16.8 mA cm^{-2}	5200 cycles at 5 mA cm^{-2} (30 min per cycle)	≈76%	[51]
Co_3O_{4-x} bubbles	6 M KOH + 0.2 M zinc acetate	806	1.84 → 1.2	961	84.3 mW cm^{-2} @80 mA cm^{-2}	800 cycles at 3 mA cm^{-2} (- min per cycle)	73%	[52]
Co/Co_2P Heterojunctions	6 M KOH + 0.2 M zinc acetate	801	1.75 → 0.97	841	321 mW cm^{-2} @550 mA cm^{-2}	200 cycles at 20 mA cm^{-2} (210 min per cycle)	62%	[47]

regulation, defect modification, ion doping, and electrochemical activation. The main goal of these approaches is to enhance the reactivity of the electrode materials and improve the overall performance of the battery.

By optimizing the microstructure of the electrode surface, the specific surface area can be increased, providing more reactive sites and improving the ion and electron transport pathways. This optimization not only facilitates the penetration of the electrolyte into the electrode but also enhances the kinetics of the electrochemical reactions, significantly improving the rate capability of the battery.[18] Several nanostructure designs of cobalt-based active materials have already been reported in the literature, including nanowire clusters, nanosheets, and 3D layered structures.[19] These innovative structural designs have shown excellent electrochemical performance. Tan et al. synthesized a porous Co_3O_4 nanowire electrode grown on a nickel foam substrate via a hydrothermal method and conducted in-depth studies on the effects of key parameters (such as temperature, reaction time, etc.) during the hydrothermal process on the electrode morphology.[12] The results showed that the electrode with a heterogeneous porous nanowire structure (**Figure 2**a,b) exhibited the largest electrochemical surface area, with a discharge capacity of up to 230 mAh g^{-1} and an active material utilization rate of 51.6% (Figure 2c,d). Moreover, it can operate ≈3000 cycles with a capacity retention ratio of 68% (Figure 2e). Mai et al. successfully prepared a binder-free cathode material grown on carbon cloth using a two-step hydrothermal method.[20] This method first grew $Co(CO_3)_{0.5}(OH)_x{\cdot}0.11H_2O$ (CCH) nanowires on the carbon cloth, followed by the uniform growth of $CoMoO_4$ (CMO) nanosheets on their surface, forming a unique 3D branched nanostructure. The synergistic effect between CCH and CMO greatly improved the conductivity of the electrode. The Zn–Co battery using this electrode achieved a discharge capacity of 256.6 mAh g^{-1} at a current density of 0.36 A g^{-1}, with an active material utilization rate of 57.5%.

Introducing oxygen vacancies has been widely confirmed as an effective method for enhancing the capacity and rate performance of Co_3O_4 electrode materials. This approach changes the electronic structure and surface properties, thereby enhancing its intrinsic conductivity and the kinetics of the redox reactions. Oxygen vacancies not only serve as active sites for redox reactions but also promote an increase in the electrochemical reaction rate.[21] Lu et al. developed an oxygen-deficient ultrathin Co_3O_4 nanosheet cathode material.[22] After introducing oxygen vacancies, the charge transfer impedance of the material was significantly reduced, accelerating electron transport. Moreover, the redox reactions of cobalt oxide have a crucial impact on the adsorption of OH^-. Density functional theory (DFT) calculations showed that the introduction of oxygen vacancies drastically reduced the adsorption energy of OH^- to −4.44 eV, which is much lower than that of the defect-free surface at −2.97 eV. This indicates that oxygen vacancies not only facilitate the kinetics of redox reactions but also serve as preferential adsorption sites for OH^-, thereby significantly improving the efficiency of the electrochemical reaction. Thanks to the optimized conductivity and redox reaction kinetics, the Zn–Co battery using this electrode achieved a high discharge specific capacity of 240.8 mAh g^{-1} at a current density of 0.525 A g^{-1}.

Introducing different cation doping into transition metal oxides can effectively adjust their lattice structure and electronic configuration, thereby enhancing the material's conductivity and ion transport rate. The doped cations form point defects in the lattice, such as doping sites or vacancies, which not only serve as active sites but also help optimize ion transport pathways.[23] Yao et al. doped Zn^{2+} into Co_3O_4 nanowires, causing the electrode material to transition from an insulator to a metal.[24] DFT calculations indicated that Co^{2+} and Co^{3+} ions occupy tetrahedral and octahedral positions, respectively. The original Co_3O_4, due to its inert nature, exhibited insulating properties, but after Zn^{2+} doping, Co^{2+} and Co^{3+} ions were substituted, and the lattice structure was distorted, significantly improving the material

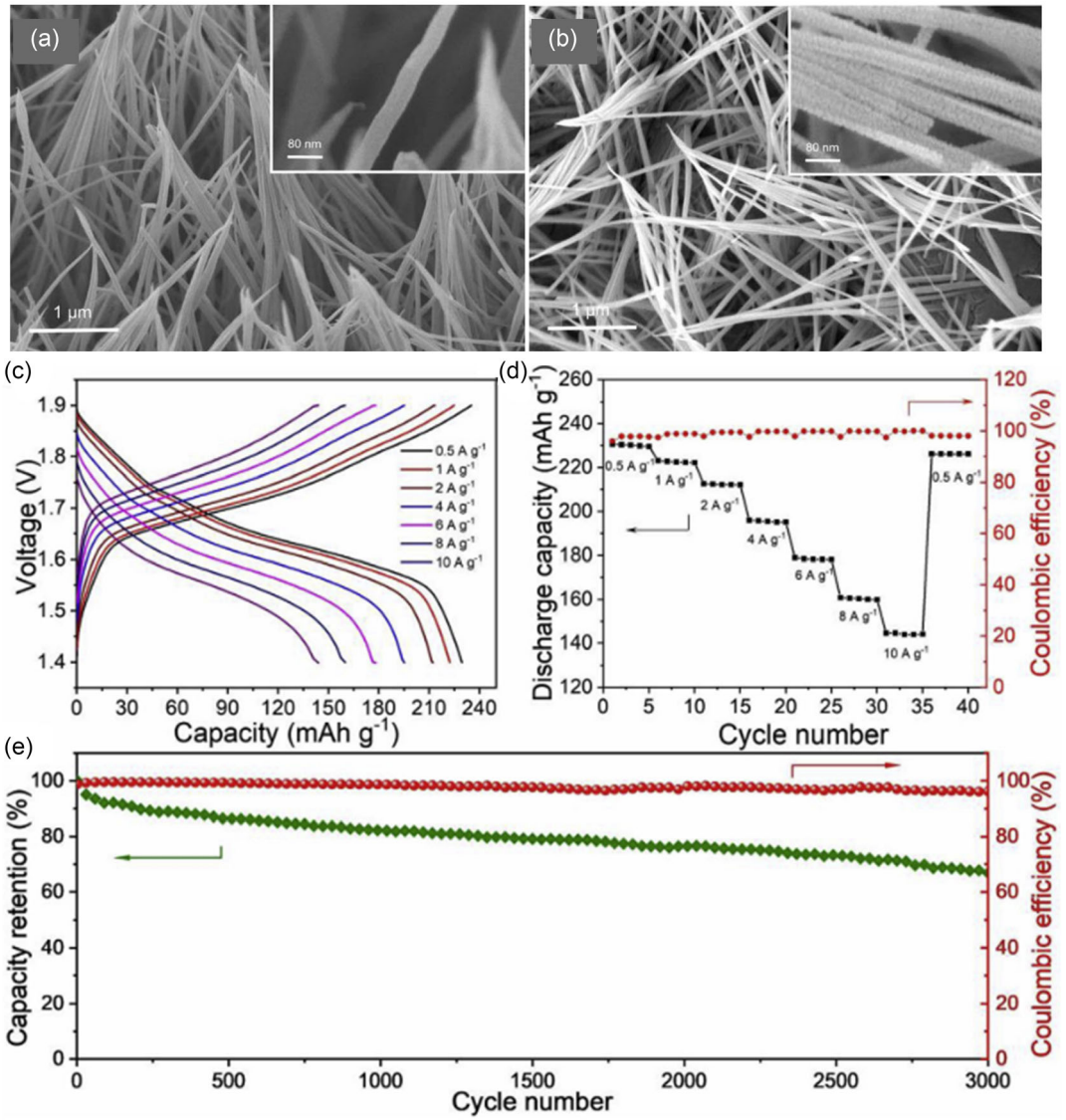

Figure 2. The porous Co_3O_4 nanowire electrodes grown on a nickel foam substrate and their battery performance: a,b) Scanning electron microscope (SEM) images of Co_3O_4 nanowire electrodes at different calcination temperatures, a) 300 °C, b) 350 °C. c) The charge–discharge voltage curves at various current densities from 0.5 to 10 A g^{-1}; d) the operating capacity and Coulombic efficiency at various current densities, and e) the capacity retention and Coulombic efficiency at various cycling numbers. Reprinted with permission.[12] Copyright 2020, Elsevier.

conductivity. Additionally, during the substitution of Co^{3+} by Zn^{2+}, oxygen vacancies were created in the lattice, providing more active sites for electrochemical reactions, which further enhanced the material's electrochemical performance.

In addition, introducing other heteroatoms into electrode materials can also effectively improve their conductivity and promote reaction kinetics, thereby enhancing electrochemical performance. Among these heteroatoms, fluorine (F) is considered an ideal dopant due to its high electronegativity. F^- ions, with an ionic radius similar to that of O^{2-} ions, can partially replace oxygen sites in metal oxide lattices. Therefore, F doping can significantly influence the redox reaction kinetics of the metal oxide/hydroxide host by adjusting the electronic or phase structure. It enhances the ionicity of the metal–F bond, resulting in higher lattice energy and reduced polarization, which improves electrochemical performance. Zhi et al. employed an F-doping strategy to enhance the cycling stability of nickel–cobalt carbonate hydroxide (NiCo-CH) cathodes (**Figure 3**a).[25] The high electronegativity of F led to significant improvements in the phase structure, morphological stability, and conductivity of NiCo-CH-F (F-doped NiCo-CH) (Figure 3b). In addition, the newly introduced phase interfaces and amorphous microdomains further enhanced the electrochemical performance of the cathode. As a result, the NiCo-CH-F electrode maintained 64% of its capacity at a current density of 8 A g^{-1} and exhibited a discharge capacity of up to 245 mAh g^{-1}.

Electrochemical activation, as another effective strategy to enhance electrode performance, can in situ reconstruct the electrode surface, alter the crystal structure, or form new surface phases, thereby increasing the number and accessibility of active sites and promoting ion and electron transport. During the electrochemical activation process, defects such as vacancies or

Perspective
doi.org/10.1002/batt.202500135
Chemistry Europe
European Chemical Societies Publishing

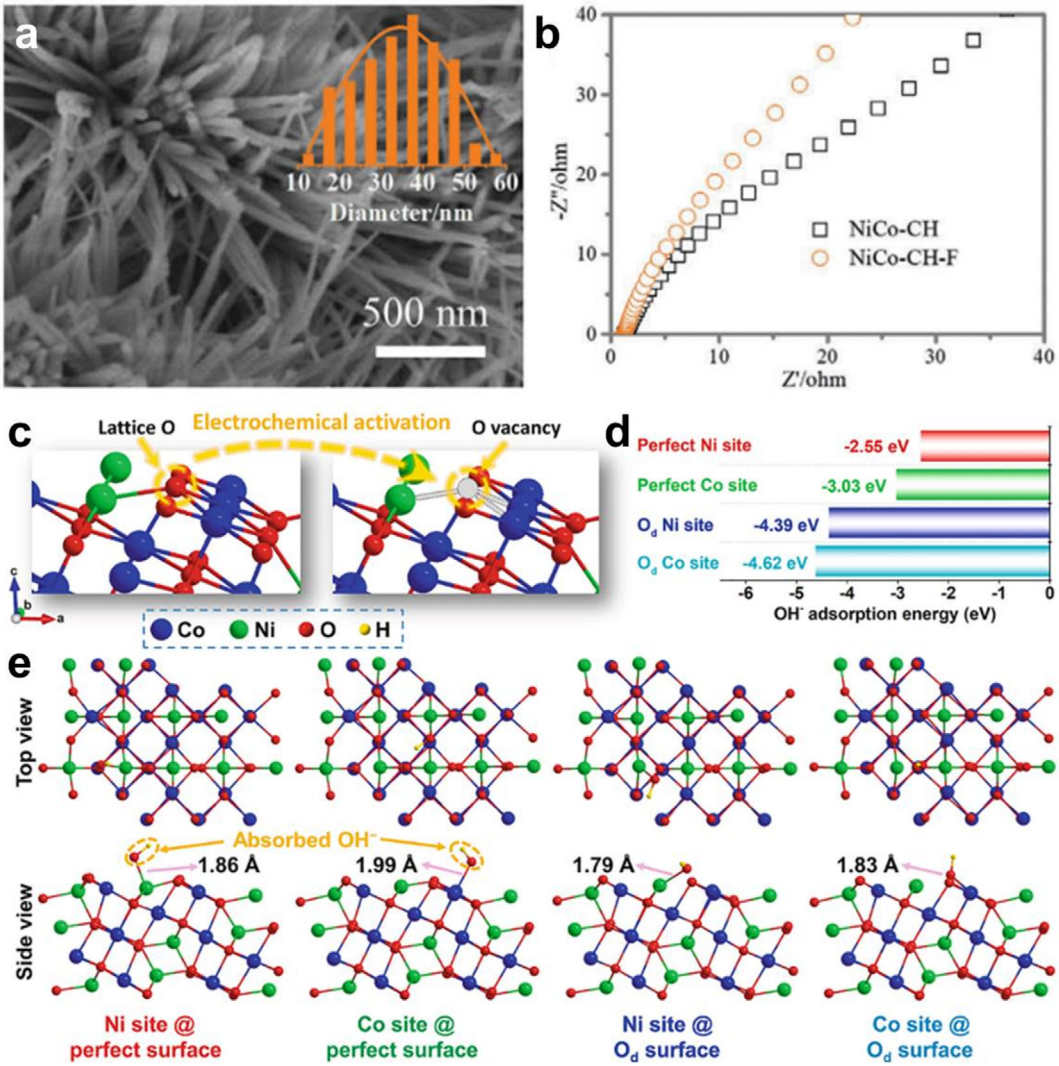

Figure 3. a) SEM image and b) Electrochemical impedance spectroscopy (EIS) curves of NiCo–CH. Reprinted with permission.[25] Copyright 2020, Wiley. c) Density functional theory (DFT) crystal models of defect-free $NiCo_2O_4$ and Od-$NiCo_2O_4$, d) distance between metal atoms and OH^-, the analysis of OH^- adsorption properties, e) comparison of OH^- adsorption energy on defect-free and Od surfaces of metal atoms. Reprinted with permission.[27] Copyright 2023, Elsevier.

doping sites can also be introduced, which serve as additional active sites and further accelerate the kinetics of electrochemical reactions.[26] Yan et al. developed a rapid and controllable electrochemical activation method that significantly enhanced the electrochemical performance of $NiCo_2O_4$ electrodes.[27] This method involved applying constant voltage treatment to $NiCo_2O_4$ electrodes in a 1 M KOH solution, which weakened the Co—O bond coordination and induced in situ reconstruction of the $NiCo_2O_4$ lattice, forming a large number of oxygen vacancies (octahedral Co^{2+}) (Figure 3c). These oxygen vacancies, acting as shallow donors, significantly improved the electron transport rate and increased the number of active sites for electrochemical reactions, thereby synergistically enhancing the reaction kinetics. DFT calculations showed that there is a significant difference in OH^- adsorption performance on the (311) crystal plane of defect-free and oxygen-deficient $NiCo_2O_4$ (Figure 3d,e). The oxygen-deficient surface exhibited lower adsorption energy and shorter adsorption distance for OH^-, indicating stronger adsorption capability and better stability, which in turn reduced the charge transfer energy barrier for redox reactions. Electrochemical impedance spectroscopy further confirmed that the charge transfer resistance of oxygen-deficient $NiCo_2O_4$ (0.55 Ω) was significantly lower than that of defect-free $NiCo_2O_4$ (1.15 Ω), and the higher slope in the low-frequency region also indicated smaller ion diffusion resistance. These characteristics enabled the oxygen-deficient $NiCo_2O_4$ electrode to achieve a nearly fivefold increase in discharge capacity (418.9 mAh g^{-1}) at a current density of 1 A g^{-1} compared to the original electrode, and it demonstrated high energy density (682.4 Wh kg^{-1}) and maximum power density (50.8 kW kg^{-1}).

2.2. Catalytic Performance Optimization

To improve the activity of transition metal compounds in oxygen catalysis and reduce the overpotential of Zn–air batteries,

researchers have proposed a series of strategies to optimize electrode materials, including carbon support, structural design, and defect engineering.[28] These methods enhance electrochemical reaction kinetics by increasing the number of reactive sites and promoting the transport of substances and electrons, thereby improving oxygen catalysis efficiency.

Enhancing the conductivity of transition metal compounds is an important research area. One common strategy is to load or grow these catalysts on carbon-based materials such as carbon nanotubes (CNTs) and porous carbon.[29] These carbon materials not only possess high conductivity but also have a large specific surface area, which helps improve the electron transfer capability of the catalyst and increases the density of active sites.[30] For example, Wang et al. successfully synthesized a catalyst by pyrolyzing graphene with a supramolecular complex, consisting of cobalt nanoparticles embedded in nitrogen-doped graphene (**Figure 4**a–c).[31] This nitrogen-doped graphene has abundant defects, which not only enhance the conductivity of the catalyst but also provide a large number of active sites. In electrochemical tests, the catalyst demonstrated excellent ORR activity ($E_{1/2} = 0.864$ V) and OER activity ($j_{10} = 383$ mV). When applied to Zn–air batteries, it exhibited a peak power density of up to 205 mW cm^{-2} and showed stable cycling performance of 667 h. Additionally, Lin et al. developed a bifunctional catalyst, encapsulating ultrafine FeNi alloyed nanoparticles in nitrogen-doped carbon nanosheets.[32] The Zn–air battery based on this catalyst achieved a peak power density of up to 162 mW cm^{-2} at a current density of 5 mA cm^{-2} and demonstrated stable cycling performance for up to 1100 h.

Structural design is a key method to optimize oxygen catalyst performance. By rationally controlling the structure of the catalyst, the effective surface area can be significantly increased, allowing more reactive sites to be accommodated and improving the efficiency of mass and electron transport. In metal–carbon hybrids, anchoring nanoscale metal particles onto carbon substrates ensures sufficient catalyst surface contact and promotes charge transfer. However, metal particles may aggregate during synthesis, requiring the design of 1D or 2D carbon nanostructures to promote the uniform dispersion of metal particles and further enhance the catalyst's performance. Shao et al. developed a catalyst composed of 3D Fe–Co bimetallic oxide ($FeCoO_x$) particles grown on nitrogen-doped graphene (N–G) (Figure 4d–f).[33] This

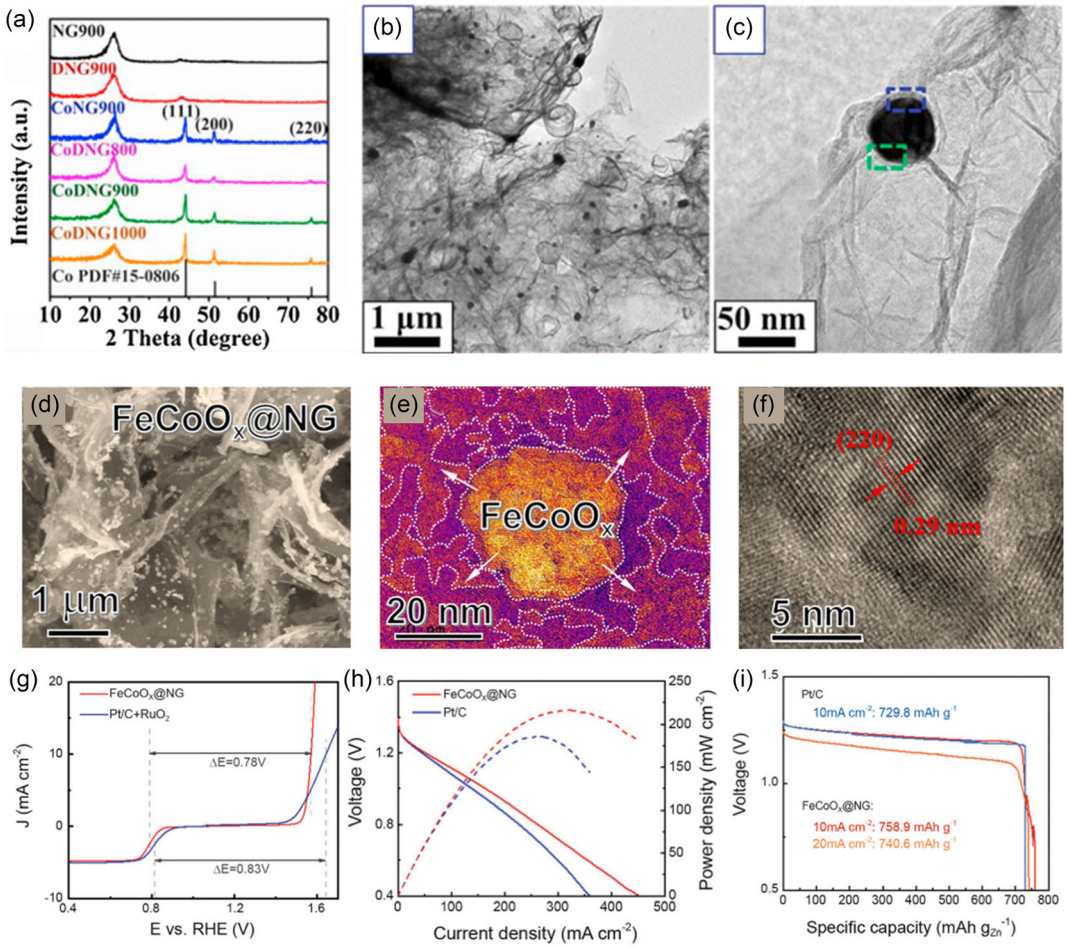

Figure 4. SEM images of a) NG, b) ZIF-67, c) ZIF-67@NG. Reprinted with permission.[31] Copyright 2021, Wiley. d) $FeCoO_x$@NG. e) Colorized TEM image of $FeCoO_x$@NG. f) High-resolution TEM image of $FeCoO_x$@NG. g) The overall linear sweep voltammetry (LSV) curves of $FeCoO_x$@NG and the mixture of Pt/C + RuO_2. h) Discharge polarization curves and corresponding power density curves of Zn–air battery based on $FeCoO_x$@NG. i) Discharge capacity curves of Zn–air battery based on $FeCoO_x$@NG at different current densities. Reprinted with permission.[33] Copyright 2023, Wiley.

catalyst not only ensures good dispersion of the metal particles but also improves the transport efficiency of O_2 and OH^- by alleviating the stacking of N–G layers, exhibiting excellent performance in electrocatalytic reactions with a $\Delta E = 0.78$ V, high power density of 215 mW cm^{-2}, and discharge capacity of 758.9 mAh g^{-1}@10 mA cm^{-2} (Figure 4g–i). By further constructing a 3D porous structure, it better facilitates the transport of electrolytes and gases and provides more catalytic active sites.[34]

Defect engineering is a strategy that introduces oxygen vacancies or heteroatoms to adjust the charge distribution of the catalyst, thereby enhancing catalytic activity. Oxygen vacancies improve the conductivity of the catalyst by stimulating electron delocalization effects. Surface etching is a common method for introducing defects, including ammonia treatment, plasma etching, and ball milling.[35] Yang et al. employed plasma treatment to introduce oxygen vacancies into cobalt oxide (Co_3O_{4-x}) nanosheets, providing a large number of active sites.[36] Zn–air batteries based on this material exhibited excellent cycling performance, lasting more than 150 h at a current density of 5 mA cm^{-2}, with an OER overpotential lower than that of commercial IrO_2. Additionally, heteroatom doping is another common method for introducing defects. Elements such as nitrogen (N), sulfur (S), or phosphorus (P) are typically incorporated to modify the electronic structure of carbon materials and optimize catalytic performance. Zhang et al. developed a 3D carbon nanosheet (CoCNTs/PNAs) catalyst using a self-assembly pyrolysis method.[37] The electronic structure of cobalt metal sites was regulated through nitrogen doping, effectively lowering the energy barriers for ORR and OER reactions. This catalyst exhibited a peak power density of up to 371.6 mW cm^{-2} in Zn–air batteries and demonstrated cycle stability for over 2000 h.

2.3. Reaction Interface Design

The optimization of the reaction interface is considered an effective approach to improving the charge–discharge performance and stability of hybrid Zn–air batteries. By enhancing the wettability of the electrode, optimizing gas transport channels, and designing the electrode structure rationally, the interface properties of the electrode can be significantly improved.[38] These strategies help to enhance the contact between the electrode, electrolyte, and gas, promoting the efficient transport of ions and electrons, thereby improving the overall electrochemical performance of the battery.

The low solubility of oxygen in the electrolyte limits the entry of gaseous reactants, negatively impacting the performance of Zn–air batteries.[39] To address this issue, hydrophobic additives, such as polytetrafluoroethylene (PTFE), are widely used in the cathode materials of Zn–air batteries to improve gas transport channels and the construction of the three-phase reaction interface, thereby accelerating the gas transport and reaction rate.[40] Ni et al. treated Co_3O_4 nanosheet electrodes using an impregnation method and studied their performance under different wettability conditions.[14] As the hydrophobicity increased, the gas transport channel and three-phase interface formed, leading to an initial increase in discharge voltage. However, excessive hydrophobic treatment resulted in the coverage of active sites, ultimately leading to a decrease in discharge voltage, and both the voltage and capacity of the Zn–Co reaction decreased with increased hydrophobicity. Ultimately, the optimized electrode, after two rounds of impregnation, showed the best performance, with a maximum power density of 31.9 mW cm^{-2}, an energy density of up to 936 Wh kg^{-1}, and stable operation over 400 charge–discharge cycles within the voltage range of 2.01 and 0.94 V, demonstrating good cycling stability. However, the aggregation of PTFE nanoparticles during the impregnation process still affected the ion and electron transport efficiency of the electrode. To address this, Tan et al. proposed an improved hydrothermal method.[41] Using this method, PTFE nanoparticles were evenly distributed on the surface and in the gaps of Co_3O_4 nanowires, effectively ensuring more active surfaces came into contact with the electrolyte and optimizing the two-phase and three-phase reaction interfaces. The Zn–air battery using electrodes treated with this hydrothermal method achieved a peak power density of 51.7 mW cm^{-2}, and the battery demonstrated good rate performance and stability within a current density range of 1–5 mA cm^{-2}. Especially at a high current density of 10 mA cm^{-2}, the battery operated stably for 100 cycles, with only an 86 mV increase in voltage difference.

In traditional Zn–air battery designs, the oxygen catalysis layer is typically covered on the air side with a gas diffusion layer made from materials like porous carbon work. The role of this layer is to facilitate the uniform distribution and transport of gas. However, there is an unmatched and disordered reaction interface between the catalyst layer and the gas diffusion layer, which limits the oxygen catalysis reaction kinetics and affects the battery's performance. To address this, Chen et al. proposed an innovative wood-derived electrode structure.[42] This electrode successfully integrates active materials, current collectors, and continuously oriented three-phase reaction interface channels, achieving the fusion of the gas diffusion layer and the catalyst layer, thus eliminating the need for an additional gas diffusion layer in traditional batteries (**Figure 5**a,b). The surface of this electrode, by loading a hydrophilic mixture of cobalt–nickel sulfides and hydroxides (CNSOH) on the wood substrate, constructs a continuous directional channel with asymmetric wettability (Figure 5c). In the electrode, the hydrophilic part forms more two-phase interfaces, while the hydrophobic part forms a rich three-phase interface (Figure 5d). This design effectively enhances the permeability of the electrolyte and the diffusion rate of oxygen, significantly improving the oxygen catalysis reaction kinetics within the electrode. The hybrid Zn–air battery using this wood-derived electrode demonstrated a specific capacity of 656.5 mAh g^{-1} in the working voltage range, a high energy density of 644.7 Wh kg^{-1}, and excellent cycling stability.

The optimization of electrode structure is considered an effective method to enhance the performance of the electrode reaction interface.[43] In hybrid Zn–air batteries, the Zn metal reaction segment requires high hydrophilicity to accelerate the transport of ions in the electrolyte and improve the electrochemical reaction rate. On the other hand, the Zn–air reaction segment requires strong hydrophobicity to promote gas diffusion and provide more reactive sites for oxygen molecules, thereby improving

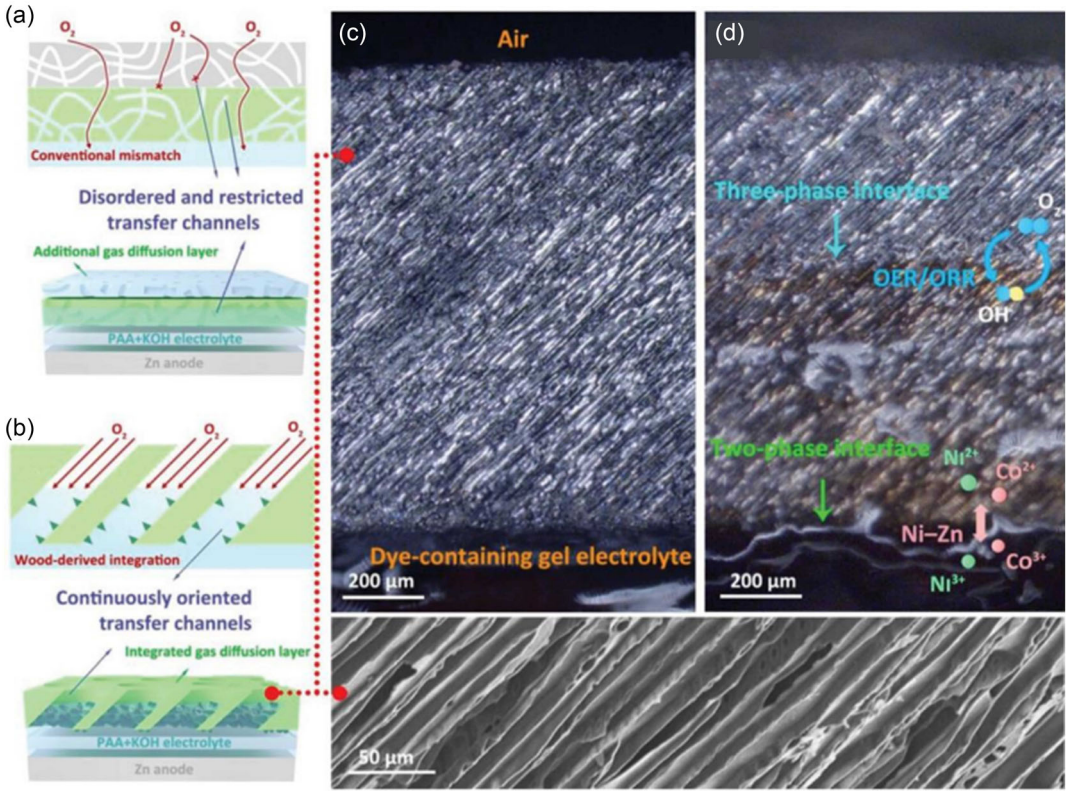

Figure 5. a) Traditional three-phase interface channel with incomplete matching and disordered transport characteristics. b) Continuous oriented three-phase interface channel with 1D directional transport characteristics, c,d) Electrolyte (c) before penetration and (d) after penetration in the continuous oriented three-phase interface channel. Reprinted with permission.[42] Copyright 2023, Wiley.

the kinetics of the ORR. Since these two reaction segments have different wettability requirements, coordinating the differences between them has become a challenge in electrode design. To address this issue, Janus electrodes, an innovative type of electrode with dual surface properties, offer an effective solution. This electrode has different wettability characteristics on the same surface, allowing a single electrode to meet the distinct wettability requirements of both reactions.[44] Zhuang et al. successfully applied Janus electrodes in Zn–air batteries to satisfy the differing wettability requirements for ORR and OER.[45] The electrode was prepared using a rolling process and divided into two parts: one side is a porous, superhydrophobic OER layer, while the other side is a dense, superhydrophobic ORR layer. In the OER segment, the superhydrophilic OER layer promotes the rapid expulsion of gas bubbles and ensures good contact with the electrolyte through its larger pore structure, effectively reducing the internal resistance of the battery. In the ORR segment, the superhydrophobicity of the ORR layer ensures good gas contact while its dense structure prevents electrode wetting and electrolyte leakage. Zn–air batteries using the Janus electrode demonstrated excellent electrochemical performance. The charge–discharge voltage difference of the battery was only 0.78 V, and it exhibited over 750 h of stable performance (around 1100 cycles) in continuous charge–discharge cycling, showing excellent long-term operational stability and durability. Through this structural design, the Janus electrode effectively resolved the conflict in wettability requirements between the two reaction segments, significantly enhancing the overall performance of the battery.

Although the asymmetric wettability design has achieved significant results in optimizing the Zn–air reaction, it has not fully considered the performance improvement of the Zn metal reaction. Shao et al. proposed an innovative electrode functional separation design strategy aimed at comprehensively optimizing the overall performance of hybrid Zn–air batteries.[46] This design, similar to the Janus electrode, resolves the conflict between electrolyte and gas accessibility in traditional single-layer electrodes by distributing different functional regions of the battery on both sides of the electrode. Specifically, on the air-facing side of the electrode, the research team used a hydrophobic MnS layer modified with Ni–Co–S nanoclusters, which significantly improved the oxygen catalytic reaction activity and gas transport rate. On the electrolyte-facing side of the electrode, a highly hydrophilic $NixCo_{1-x}S_2$ layer was employed. This design not only enhanced the cationic redox performance of the Zn metal reaction but also accelerated ion transport between the electrode and the electrolyte. With this functional separation design, the hybrid Zn–air battery demonstrated exceptional electrochemical performance. At a current density of 5 mA cm^{-2}, the charge–discharge voltage difference was only 635 mV, with an energy efficiency of up to 74%. After 200 cycles (≈200 h), the battery still maintained 68% of its high energy efficiency. Furthermore, at a current density of 100 mA cm^{-2}, the battery's power density reached

153 mW cm^{-2}, ≈50% higher than that of traditional Pt/C + IrO_2 electrodes. This design significantly improved the battery's energy efficiency, rate capability, and cycle stability, providing a new approach for optimizing the performance of hybrid Zn batteries.

Inspired by the hierarchical structure of wheat, Xu et al. developed densely aligned Co/Co_2P heterostructures grown on the "central stalk" of P/N codoped carbon nanofibers (Co/Co_2P@PNCF).[47] This biomimetic nanostructure not only provides abundant exposed active sites to maximize accessibility but also establishes an efficient multichannel network for electron transfer and O_2/OH^- diffusion. As shown in **Figure 6**a, the electrode exhibits a contact angle of 128°, where the P/N codoped carbon effectively enhances surface hydrophobicity, facilitating gas trapping at micro-/nanointerfaces. During the OER, O_2 bubbles rapidly spread across the Co/Co_2P@PNCF electrode within merely 50 ms, significantly faster than those observed on the other two electrode architectures (2 s and 6 s, Figure 6b). Consequently, compared to hydrophilic counterparts, this electrode demonstrates enhanced O_2 adsorption and accelerated O_2 transport. The P/N codoped carbon and CNTs function analogously to wheat seeds and awns, synergistically capturing oxygen from oxygen-saturated electrolytes (Figure 6c), thereby improving oxygen diffusion across the catalyst surface. When assembled into a hybrid battery, the system displays a dramatically reduced discharge–charge voltage gap and substantially enhanced discharge current, achieving a peak power density of 321 mW cm^{-2} (Figure 6d). Furthermore, it delivers an exceptional specific capacity of 801 mAh g_{Zn}^{-1} and a high energy density of 841 Wh kg_{Zn}^{-1} at a current density of 20 mA cm^{-2} (Figure 6e).

In practical applications, high discharge capacity is crucial for battery performance. When the actual capacity is high, the contribution of the low proportion of high-voltage sections in hybrid batteries is very limited, making the energy efficiency close to that of pure Zn–air batteries.[48] In addition, for the positive electrodes, the active material participates in both the redox reaction of transition metals and acts as a bifunctional electrocatalyst for the Zn–air reaction. In Zn–Co batteries, the Faraday redox

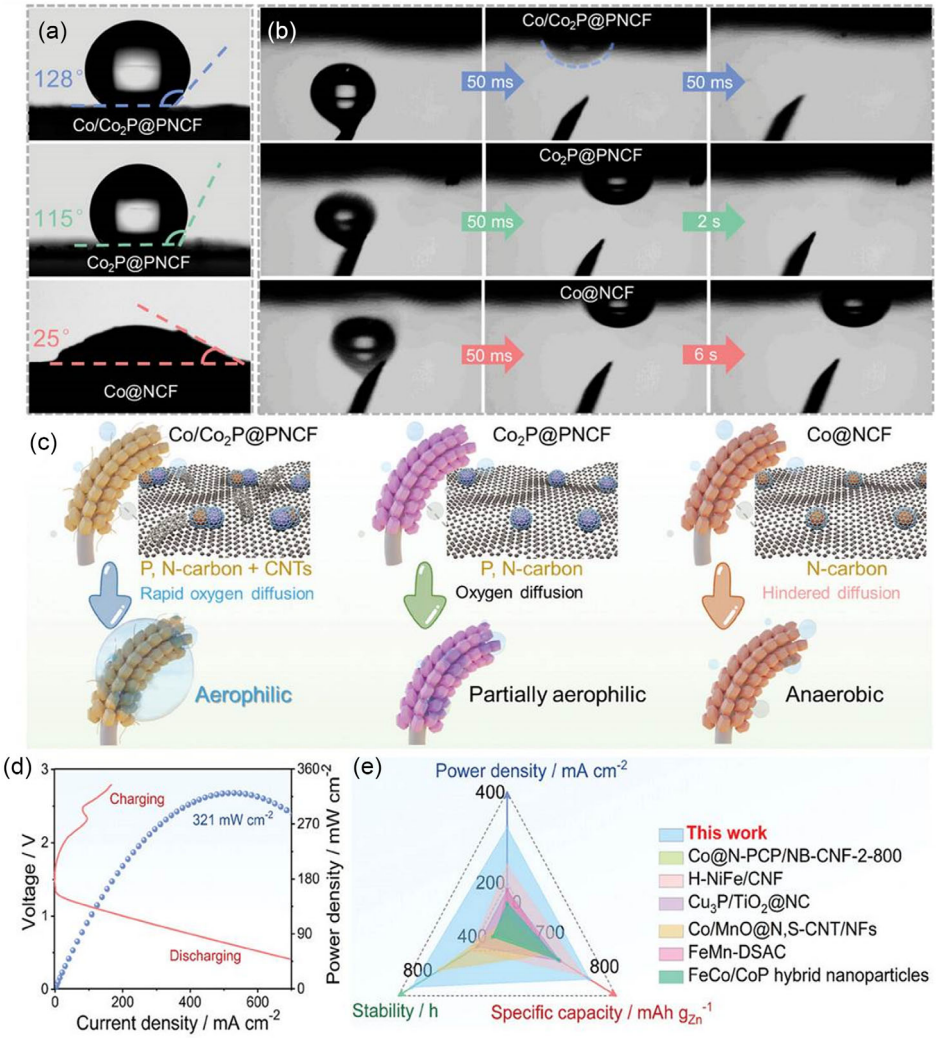

Figure 6. a) The measured surface contact angles, b) O_2 bubbles adhesion behavior evolution on the surfaces of the Co/Co_2P@PNCF, Co_2P@PNCF, and Co@NCF, c) schematic illustration of oxygen diffusion processes, d) charge–discharge and power density curves, and e) performance comparison of the hybrid batteries. Reprinted with permission.[47] Copyright 2025, Wiley.

reaction requires high hydrophilicity to promote ion transport at the solid/liquid interface. On the other hand, the ORR/OER in Zn–air batteries requires high hydrophobicity to construct gas transport channels and more three-phase interfaces to achieve efficient utilization of catalysts. Traditional electrodes usually use hydrophobic additives to achieve hydrophobicity, but the additives will cover the surface of the active material, resulting in a significant decrease in its actual utilization rate. Therefore, the simultaneous optimization of the two reactions through interface engineering is the key to achieving high area capacity and energy efficiency.

3. Summary and Perspective

The hybrid Zn–Co/air battery bridges the high capacity of Zn–air batteries with the high voltage of Zn–Co batteries, achieving synergistic optimization of high energy density, high energy efficiency, long cycle life, and environmental friendliness in a single cell, demonstrating broad application prospects. However, the cathode material system still faces several critical challenges that severely hinder its practical development. In recent years, researchers have made significant progress in improving active material utilization, optimizing oxygen catalytic performance, and designing three-phase interfaces, which have notably enhanced the electrochemical performance of the battery. To further improve the performance of hybrid Zn–Co/air batteries and accelerate their commercialization, future research should focus on the following three aspects.

First, the positive electrode materials still require further optimization. On the one hand, the air reaction segment is restricted by oxygen catalytic activity. Although combining transition metal composites with conductive carbon materials effectively enhances electrical conductivity, the agglomeration of nanoparticles has not been significantly alleviated, leading to insufficient active sites and reaction heterogeneity. Simultaneously, low porosity hinders mass transport within the electrode. Thus, it is necessary to construct appropriate carbon-based matrices to improve catalytic activity and mass transfer rates. On the other hand, for the cobalt-based reaction segment, the loading is typically limited to 1–2 mg cm^{-2} to enhance mass transport, severely restricting areal energy density. Thick electrodes based on gradient structural designs could be applied to improve active material utilization and catalytic performance. Methods such as gradient electrodes, vertical channels, porosity regulation and other structural designs, self-activated multilevel structures, and porous skeleton optimization design can be adopted.

Second, the dendrite and passivation of the Zn electrode should also be concerned, and some optimization strategy can be adopted. Structural optimization (such as 3D porous zinc electrodes) can achieve uniform current distribution, inhibit dendrite growth, and delay passivation; alloying can adjust surface charge distribution, increase hydrogen evolution overpotential, and inhibit dendrites and corrosion; interface modification (such as Al_2O_3 inorganic coating or anion exchange membrane organic coating) can isolate zinc from direct contact with the electrolyte and reduce side reactions; electrolyte optimization (such as adding ZnO or Li^+ ions) can also adjust the zincate concentration and inhibit the formation of the passivation layer.

Third, the unmatched reaction interfaces in hybrid Zn batteries should be addressed. The significantly different charge/discharge voltage plateaus for Zn–Co and Zn–air reactions necessitate optimized allocation ratios for overall performance. In the current research, due to the application of Zn plate with excess mass loading, the areal capacity contribution from the high-voltage Zn–Co segment remains limited, resulting in similar energy efficiency to the conventional Zn–air batteries. Therefore, designing an appropriate negative/positive (N/P) capacity ratio is critical to achieving optimal energy density and efficiency.

Fourth, the mass transport mechanisms at the reaction interface require in-depth investigation. The positive electrode of hybrid Zn–Co/air batteries involves multiphase transport of ions (OH^-) and gases (O_2). Key parameters such as electrode porosity, interfacial wettability, and reaction interface structure significantly influence mass transport. However, existing research is yet to systematically quantify these parameters. A comprehensive understanding of internal mass transfer mechanisms through multiphysics coupling models (e.g., integrating Nernst–Planck equations with Butler–Volmer kinetics) is urgently needed to provide theoretical guidance for optimizing three-phase interfaces.

Fifth, the application scenarios demand further exploration. Hybrid Zn–Co/air batteries combine the dual advantages of Zn–air and Zn–Co systems, enabling operation in both oxygen-rich and oxygen-free environments, which overcomes the application limitations of traditional air batteries. Given their unique dual-mode operation, emphasis should be placed on exploring their potential in specialized scenarios (e.g., high-altitude military equipment, deep-sea exploration devices, and wearable electronics) and assessing their stable energy supply capabilities. By strategically aligning the characteristics of the two-stage charge/discharge reactions, the performance advantages of these batteries can be maximized, paving new pathways for commercialization.

Breakthroughs in these research directions will provide critical theoretical support for optimizing the performance of hybrid Zn–Co/air batteries, lay the foundation for developing next-generation Zn-based energy storage systems, and promote their commercialization in specific application scenarios, thereby enhancing market competitiveness.

Acknowledgements

W.S. thanks the funding support from Anhui Provincial Natural Science Foundation (2408085QE177) and P.T. thanks the funding support from National Innovative Talents Program (GG2090007001).

Conflict of Interest

The authors declare no conflict of interest.

Author Contributions

Wenxu Shang: conceptualization (lead); investigation (lead); writing—original draft (lead). **Yongfu Liu**: investigation (lead). **Yi He**: investigation (equal); supervision (equal); writing—review and editing (equal). **Peng Tan**: funding acquisition (lead); supervision (lead); writing—review and editing (lead).

Keywords: catalytic performances · hybrid Zn–Co/air batteries · reaction interfaces · utilizations

[1] W. Shang, W. Yu, Y. Liu, R. Li, Y. Dai, C. Cheng, P. Tan, M. Ni, *Energy Storage Mater.* **2020**, *31*, 44.
[2] H. Li, L. Ma, C. Han, Z. Wang, Z. Liu, Z. Tang, C. Zhi, *Nano Energy* **2019**, *62*, 550.
[3] Y. Shi, Y. Chen, L. Shi, K. Wang, B. Wang, L. Li, Y. Ma, Y. Li, Z. Sun, W. Ali, S. Ding, *Small* **2020**, *16*, 2000730.
[4] W. Shang, Y. Ma, P. Tan, *Adv. Funct. Mater.* **2024**, *34*, 2315782.
[5] W. Shang, W. Yu, X. Xiao, Y. Ma, Z. Chen, M. Ni, P. Tan, *Appl. Energy* **2022**, *308*, 118366.
[6] Y. Shao, W. Lu, T. Zhang, B. Yin, B. Bin Xie, J. Ning, Y. Hu, *Carbon Energy* **2025**, e701.
[7] W. Fan, C. Zhu, X. Wang, H. Wang, Y. Zhu, J. Chen, W. Tian, J. Wu, G. Yu, *Nat. Commun.* **2025**, *16*, 1273.
[8] W. Shang, W. Yu, P. Tan, B. Chen, Z. Wu, H. Xu, M. Ni, *J. Mater. Chem. A* **2019**, *7*, 15564.
[9] N. Shang, K. Wang, M. Wei, Y. Zuo, P. Zhang, H. Wang, Z. Chen, P. Pei, *J. Mater. Chem. A* **2022**, *10*, 16369.
[10] N. Xu, Y. Zhang, Y. Wang, M. Wang, T. Su, C. A. Coco, J. Qiao, X. D. Zhou, *Appl. Energy* **2020**, *279*, 115876.
[11] W. Shang, W. Yu, X. Xiao, Y. Ma, P. Tan, M. Ni, *J. Power Sources* **2021**, *483*, 229192.
[12] W. Shang, W. Yu, X. Xiao, Y. Ma, C. Cheng, Y. Dai, P. Tan, M. Ni, *Electrochim. Acta* **2020**, *353*, 136535.
[13] W. Shang, W. Yu, X. Xiao, Y. Ma, Y. He, P. Tan, *Energy Fuels* **2022**, *36*, 1121.
[14] P. Tan, B. Chen, H. Xu, W. Cai, W. He, M. Ni, *Electrochim. Acta* **2018**, *283*, 1028.
[15] P. Ye, K. Fang, H. Wang, Y. Wang, H. Huang, C. Mo, J. Ning, Y. Hu, *Nat. Commun.* **2024**, *15*, 1012.
[16] P. Tan, B. Chen, H. Xu, W. Cai, W. He, M. Ni, *Appl. Catal. B Environ.* **2019**, *241*, 104.
[17] L. Yan, J. Chen, C. Yang, J. Ning, Y. Hu, *Small Sci.* **2024**, *4*, 2300094.
[18] Y. Li, Z. Wang, Y. Cai, M. E. Pam, Y. Yang, D. Zhang, Y. Wang, S. Huang, *Energy Environ. Mater.* **2022**, *5*, 823.
[19] S. Zhang, B. Yin, Y. Luo, L. Shen, B. Tang, Z. Kou, X. Liu, D. Lim, D. Gu, Z. Wang, H. Gong, *Nano Energy* **2019**, *68*, 104314.
[20] M. Li, J. Meng, Q. Li, M. Huang, X. Liu, K. A. Owusu, Z. Liu, L. Mai, *Adv. Funct. Mater.* **2018**, *28*, 1802016.
[21] D. Wang, S. Zhang, C. Li, X. Chen, W. Zhang, X. Ge, H. Lin, Z. Shi, S. Feng, *Small* **2022**, *18*, 2105970.
[22] Y. Lu, J. Wang, S. Zeng, L. Zhou, W. Xu, D. Zheng, J. Liu, Y. Zeng, X. Lu, *J. Mater. Chem. A* **2019**, *7*, 21678.
[23] X. Hu, G. Luo, X. Guo, Q. Zhao, R. Wang, G. Huang, B. Jiang, C. Xu, F. Pan, *Sci. Bull.* **2021**, *66*, 708.
[24] Q. Li, Q. Zhang, Z. Zhou, W. Gong, C. Liu, Y. Feng, G. Hong, Y. Yao, *Nano Res.* **2021**, *14*, 91.
[25] X. Li, Y. Tang, J. Zhu, H. Lv, L. Zhao, W. Wang, C. Zhi, H. Li, *Small* **2020**, *16*, 2001935.
[26] C. Yang, W. Zhong, K. Shen, Q. Zhang, R. Zhao, H. Xiang, J. Wu, X. Li, N. Yang, *Adv. Energy Mater.* **2022**, *12*, 2200077.
[27] Y. Zhang, D. Sun, Y. Wang, X. Liu, H. Sun, T. Cai, X. Li, H. Hu, X. Zhang, W. Xing, Z. Yan, *Chem. Eng. J.* **2023**, *453*, 139736.
[28] L. Yan, B. Xie, C. Yang, Y. Wang, J. Ning, Y. Zhong, Y. Hu, *Adv. Energy Mater.* **2023**, *13*, 2204245.
[29] Y. Wang, J. Liu, T. Lu, R. He, N. Xu, J. Qiao, *Appl. Catal. B Environ.* **2023**, *321*, 122041.
[30] W. Zhang, X. Guo, C. Li, J. Y. Xue, W. Y. Xu, Z. Niu, H. Gu, C. Redshaw, J. P. Lang, *Carbon Energy* **2023**, *5*, e317.
[31] A. Wang, C. Zhao, M. Yu, W. Wang, *Appl. Catal. B Environ.* **2021**, *281*, 119514.
[32] X. Li, Y. Liu, H. Chen, M. Yang, D. Yang, H. Li, Z. Lin, *Nano Lett.* **2021**, *21*, 3098.
[33] Z. Zheng, C. Wang, P. Mao, Y. Zhu, R. Ran, W. Zhou, K. Liao, Z. Shao, *Carbon Energy* **2023**, *5*, e274.
[34] H. J. Qiu, P. Du, K. Hu, J. Gao, H. Li, P. Liu, T. Ina, K. Ohara, Y. Ito, M. Chen, *Adv. Mater.* **2019**, *31*, 1900843.
[35] T. Zhou, N. Zhang, C. Wu, Y. Xie, *Energy Environ. Sci.* **2020**, *13*, 1132.
[36] M. Li, F. Luo, Q. Zhang, Z. Yang, Z. Xu, *J. Catal.* **2020**, *381*, 395.
[37] X. Shu, Q. Chen, M. Yang, M. Liu, J. Ma, J. Zhang, *Adv. Energy Mater.* **2023**, *13*, 2202871.
[38] S. Zeng, G. Duan, R. Yu, Q. Qin, S. He, S. Jiang, H. Yang, X. Han, J. Han, B. Y. Xia, *Prog. Mater. Sci.* **2025**, *147*, 101356.
[39] H. Tian, X. Cui, H. Dong, G. Meng, F. Kong, Y. Chen, L. Peng, C. Chen, Z. Chang, J. Shi, *Energy Storage Mater.* **2021**, *37*, 274.
[40] Y. He, Z. Zhao, Y. Cui, W. Shang, Y. Chen, P. Tan, *Energy Storage Mater.* **2023**, *57*, 360.
[41] W. Shang, W. Yu, Y. Ma, Y. He, Z. Zhao, M. Ni, H. Zhao, P. Tan, *Adv. Mater. Interfaces* **2021**, *8*, 2101256.
[42] L. Li, Q. Cao, Y. Wu, Y. Zheng, H. Tang, J. Ge, M. Liang, B. Zhou, B. Jiang, S. Wu, F. Wang, Y. Pang, Z. Shen, C. Guan, H. Chen, *Adv. Mater.* **2023**, *35*, 2300132.
[43] M. Wu, G. Zhang, N. Chen, W. Chen, J. Qiao, S. Sun, *Energy Storage Mater.* **2020**, *24*, 272.
[44] S. Sheng, B. Shi, C. Wang, L. Luo, X. Lin, P. Li, F. Chen, Z. Shang, H. Meng, Y. Kuang, W. F. Lin, X. Sun, *ACS Appl. Mater. Interfaces* **2020**, *12*, 23627.
[45] X. Zhang, X. Wang, Z. Guan, J. Fang, R. Sui, J. Pei, Y. Qin, D. Wei, W. Zhu, Z. Zhuang, *ACS Appl. Mater. Interfaces* **2022**, *14*, 52849.
[46] Y. Zhong, X. Xu, P. Liu, R. Ran, S. P. Jiang, H. Wu, Z. Shao, *Adv. Energy Mater.* **2020**, *10*, 2002992.
[47] Z. Xu, J. Chen, T. Zhang, H. Lu, L. Yan, J. Ning, Y. Hu, *Adv. Energy Mater.* **2025**, *15*, 2402839.
[48] Y. Ma, Z. Zhao, Y. Cui, J. Yu, P. Tan, *Small* **2024**, *20*, 2308500.
[49] P. Tan, B. Chen, H. Xu, W. Cai, W. He, M. Liu, Z. Shao, M. Ni, *Small* **2018**, *14*, 1800225.
[50] L. Ma, S. Chen, Z. Pei, H. Li, Z. Wang, Z. Liu, Z. Tang, J. A. Zapien, C. Zhi, *ACS Nano* **2018**, *12*, 8597.
[51] B. Li, J. Quan, A. Loh, J. Chai, Y. Chen, C. Tan, X. Ge, T. S. A. Hor, Z. Liu, H. Zhang, Y. Zong, *Nano Lett.* **2017**, *17*, 156.
[52] H. Wang, Y. Zhou, S. Zhang, C. Deng, *Chem. Eng. J.* **2020**, *407*, 127043.

Manuscript received: February 25, 2025
Revised manuscript received: March 27, 2025
Version of record online: April 17, 2025